NASA TM X-325

TECHNICAL MEMORANDUM

X-325

FLUTTER INVESTIGATION OF

60° TO 80° DELTA-PLANFORM SURFACES

AT A MACH NUMBER OF 7.0

By Robert W. Miller and Margery E. Hannah

Langley Research Center
Langley Field, Va.

NATIONAL AERONAUTICS AND SPACE ADMINISTRATION

WASHINGTON

October 1960

NATIONAL AERONAUTICS AND SPACE ADMINISTRATION

TECHNICAL MEMORANDUM X-325

FLUTTER INVESTIGATION OF 60° TO 80° DELTA-PLANFORM SURFACES AT A MACH NUMBER OF 7.0*

By Robert W. Miller and Margery E. Hannah

SUMMARY

The flutter characteristics of a series of half-span delta surfaces which had leading-edge sweep angles ranging from 60° to 80° were investigated in helium flow at a Mach number of 7.0 in the Langley hypersonic aeroelasticity tunnel. For each value of sweep angle both wedge and double-wedge airfoil sections were tested at two pitch-axis positions. The models were mounted so that a rigid-body flapping-pitching type of flutter was encountered.

Analysis of the results and comparison with theory show that the wedge models are more stable than the corresponding double-wedge models; the pitch-axis location at or near the center of gravity is more stable than the more forward location; the effects of leading-edge sweep angle on the flutter characteristics appear to be small; and an uncoupled-mode piston-theory analysis gave the best agreement with the experimental results.

INTRODUCTION

The high dynamic pressures at hypersonic speeds make flutter a definite possibility for the aerodynamic controls and lifting surfaces of antimissile missiles and other proposed configurations. However, very little information on flutter at hypersonic speeds is available. Most of the data are given in references 1 and 2, which report the results of tests of rectangular-planform, all-movable controls at Mach numbers of 6.9 and 7.2, and references 3 and 4, which deal with specific tail surfaces at the same Mach numbers. These investigations show that flutter characteristics can be calculated for all-movable controls of rectangular and nearly rectangular planform.

The purpose of this paper is to extend the study of references 1 and 2 to highly swept delta surfaces. Experimental flutter results are presented and compared with the results of several types of theoretical flutter calculations.

The models used in the present investigation were a series of half-span delta surfaces with leading-edge sweep angles ranging from 60° to 80° and 5-percent-thick wedge or double-wedge airfoil sections. The models were mounted in such a way that the flutter mode involved rigid-body flapping and pitching motions. The tests were made at M = 7.0 in helium flow.

SYMBOLS

a	speed of sound, fps
b_r	root semichord, ft
b	local semichord, ft
c_r	root chord, ft
l	semispan, ft
M	Mach number
m	mass of model, slugs
q	dynamic pressure, lb/sq ft
R	stiffness-altitude parameter, $\frac{b\omega_\alpha}{a}\sqrt{\mu}$
r	leading-edge radius, in.
x_o	distance from leading edge to pitch axis, expressed as fraction of root chord
Λ	leading-edge sweep angle, deg
μ	mass ratio, $\frac{m}{\frac{1}{3}\pi b r^2 \rho l}$
ω_α	circular frequency in pitch, radians/sec

ρ density of test medium, slugs/cu ft

Subscripts:

calc calculated

exp experimental

APPARATUS AND PROCEDURE

Models

The models used in the present investigation were 20 half-span delta surfaces which had leading-edge sweep angles ranging from 60° to 80° in 5° increments. For each value of sweepback angle two airfoil shapes (blunted 5-percent-thick wedge and double-wedge sections) and two pitch-axis positions (60 and 65 percent root chord) were tested. Sketches of the models are presented in figure 1 and a photograph of models with the various sweep angles is shown in figure 2. Pertinent dimensions of the models, including mass and frequency characteristics, are listed in table I.

The models were constructed of a 0.048-inch-thick steel plate core with balsa wood glued to both faces to give the desired airfoil shape. Each model was supported by a beam which was cantilevered from the tunnel wall (fig. 1). The beam was integral with the steel core of the model and was 2 inches long, 1/2 inch wide, and 0.048 inch thick.

A reflection plane (see fig. 1) was used to insure that the model was in a region of uniform flow. The reflection plane was supported by a diamond-shaped fairing which shielded the beam from the airstream. The fore-and-aft location of the model on the plane changed with pitch-axis location.

All models were vibrated by use of an air-jet shaker before testing and the first four vibration modes and frequencies were determined. Nodal patterns typical of all the models are shown in figure 3. The frequencies for each model are listed in table I and are plotted against leading-edge sweep angle in figure 4. For all of the models the third and fourth frequencies, corresponding to the second bending and camber modes, were well above the first and second frequencies.

Time-exposure photographs were made of several of the models while they were vibrating in one of their natural modes. Two such photographs are shown in figure 5. The mode-shape deflections obtained from the photographs showed that, within reading error, all elastic deformation

took place in the beam during vibration at the first and second frequencies. Thus, in these two modes the model itself moved as a rigid body with flapping or pitching motion.

Tunnel

The tests were performed in the 8-inch-diameter test section of the Langley hypersonic aeroelasticity tunnel, which uses helium as a test medium. The tunnel is of the blowdown type and has a maximum dynamic pressure of about 5,500 pounds per square foot and a Mach number of approximately 7.0. Figure 6 shows the Mach number distribution across the test section with the reflection plane and model mounting fixtures in place.

A detailed description of the tunnel and a discussion of some of the characteristics of helium as a flutter testing medium are given in reference 2.

Test Procedure

The models were mounted in the test section at an angle of attack of 0°. Flow was established in the tunnel at a low dynamic pressure which was increased, while the Mach number remained constant, until the model fluttered or maximum operating conditions of the tunnel were reached. Flutter was encountered over a dynamic-pressure range of 1,700 to 4,500 pounds per square foot. Signals from strain gages mounted on the model supporting beam (see fig. 2) and tunnel stagnation temperature and pressure were recorded on an oscillograph during the test. A portion of a typical oscillograph record showing flutter is reproduced in figure 7. Motion pictures of the flutter of most of the models were also obtained.

ANALYSIS

Two-degree-of-freedom flutter calculations were made for all models by using the first two coupled or uncoupled modes (that is, the first flapping and first pitching modes) in conjunction with second-order piston theory (ref. 5) and also by using the uncoupled modes with lifting-surface theory (refs. 6 and 7). The equations of motion used in the calculations are derived, for example, in references 8 and 9.

The coupled modes used with piston theory were obtained from photographs of the vibrating models. (See fig. 5.) The mode shapes were

assumed to be orthogonal and the experimentally determined flapping and pitching frequencies given in table I were used in the solution of the flutter determinant. Generalized mass terms were calculated from the experimentally measured mass, moment of inertia about the beam axis, and center-of-gravity position as given in table I, and from the experimentally determined mode shapes. The mass of the beam was not included in these values. For the airfoil thickness terms used with piston theory for the double-wedge airfoil section, the airfoil was considered to have blunt leading and trailing edges which were the thickness of the steel plate core of the model (0.048 inch). A sample calculation which was made for sharp leading and trailing edges indicated no appreciable difference in the flutter velocity due to bluntness.

As previously discussed, the exposed section of the model vibrated as a rigid body while the elastic deformation took place in the beam. Consequently, the uncoupled modes were calculated from beam theory by assuming the system to consist of a uniform cantilever beam with a concentrated large mass and inertia located on the beam axis at the spanwise center of gravity of the model. The mass of the beam was neglected. The mass parameters and generalized masses of each model were computed by using a mass-per-unit area obtained by taking the average of the mass-per-unit area of all 20 models.

RESULTS AND DISCUSSION

The results of the tests are given in table II, which lists the experimental dynamic pressure, density, speed of sound, flutter-pitching frequency ratio, and a stiffness-altitude parameter at flutter for each run. Only one of the 20 models tested did not encounter flutter; the data given for that model are maximum tunnel conditions reached during the test. It can be seen in figure 4 that the flutter frequency always fell between the flapping and pitching frequencies. The motion pictures taken during the tests also showed that the models had a flapping-pitching type of motion during flutter.

Also presented in table II are a theoretical flutter-pitching frequency ratio and stiffness-altitude parameter for each run as computed by each of the theoretical methods previously discussed. The stiffness-altitude parameter $R = \frac{b\omega_\alpha}{a}\sqrt{\mu}$ depends only upon the physical properties of the wing - in particular, the torsion stiffness - and upon the atmosphere in which it operates. Its value increases as either altitude or stiffness increases, so that when this parameter is used as the ordinate in a plot, the stable region will normally be above the flutter boundary.

Figure 8 presents the experimental results in the form of stiffness-altitude parameter as a function of leading-edge sweep. Four curves are shown, one for each of the combinations of airfoil shape and pitch-axis location. It can be seen that the wedge models always fluttered at a lower value of stiffness-altitude parameter than the corresponding double-wedge models and are, therefore, more stable. This effect is attributed to a more rearward location of the static center of pressure. Similarly, it can be seen that the models with the pitch-axis location at 65 percent root chord are more stable than those with the pitch axis in a more forward location. This favorable effect is probably due to less coupling between degrees of freedom with the pitch axis nearer the center of gravity.

From figure 8 it appears that the stiffness-altitude parameter tends to increase with leading-edge sweep angle. However, it should be noted that there was a corresponding increase (from about 0.45 to about 0.72) of flapping-pitching frequency ratio. This can be seen in figure 9, which is a plot of both flapping-pitching and flutter-pitching frequency ratio against leading-edge sweep angle.

In order to examine more directly the effects of sweep-angle variation, the experimental values of stiffness-altitude parameter were adjusted analytically to the value they would have had if the flapping-pitching frequency ratio for all models had been the same. The adjustment was made in the following manner. A curve of theoretical stiffness-altitude parameter plotted against flapping-pitching frequency ratio was obtained for each model from the coupled-mode piston-theory calculations. A ratio of theoretical stiffness-altitude parameter at a reference frequency ratio to theoretical stiffness-altitude parameter at the actual frequency ratio was determined from this curve and the experimental stiffness-altitude parameter for that model was multiplied by this ratio. The frequency ratio for the 70° sweep-angle model from each group was arbitrarily chosen as the reference frequency ratio for that group. These adjusted values of stiffness-altitude parameter are plotted as functions of sweep angle in figure 10. These results show that although the relative position of the curves remains the same, the tendency of the stiffness-altitude parameter to increase with sweep angle has been largely removed.

Figure 11 presents a comparison of theoretical and experimental results in terms of the ratio of calculated to experimental stiffness-altitude parameter plotted against leading-edge sweep angle. The experimental data are compared with the results obtained by the three theoretical methods previously discussed. Briefly, these methods are (1) a coupled-mode analysis using piston theory for which the modes were obtained experimentally, (2) an uncoupled-mode analysis using piston theory and computed modes, and (3) an uncoupled-mode analysis using linearized lifting-surface theory and the computed modes.

Of the three calculation methods, only the uncoupled-mode piston-theory results generally indicated the same trend with leading-edge sweep angle as the experimental data. As can be seen in figure 11, the uncoupled-mode lifting-surface theory calculations gave results which were always higher than the experimental results for the models with 60° leading-edge sweep angle and always lower than the experimental for the models with 80° sweep angle. The coupled-mode piston-theory analysis may have been adversely affected by the inaccuracies involved in obtaining the mode shapes; and the linearized lifting-surface theory does not take into account the thickness effect present in the experimental results, which may be very important at hypersonic speeds.

L
1
0
1
3

CONCLUSIONS

Tests were made at a Mach number of 7.0 in helium on a series of highly swept delta surfaces having wedge or double-wedge airfoil sections. The models were mounted so that a rigid-body flapping-pitching type of flutter occurred. Analysis of the experimental results and comparison with several types of flutter calculations have resulted in the following conclusions:

1. The wedge models are more stable than the corresponding double-wedge models.

2. The models with the pitch axis at or near the center of gravity are more stable than those with the pitch axis farther forward.

3. After analytical adjustment of the experimental data to remove the effects of frequency ratio, the effects of leading-edge sweep angle on the flutter characteristics appear to be small.

4. An uncoupled-mode piston-theory analysis gave the best overall agreement with the experimental results.

Langley Research Center,
National Aeronautics and Space Administration,
Langley Field, Va., June 16, 1960.

REFERENCES

1. Runyan, Harry L., and Morgan, Homer G.: Flutter at Very High Speeds. NACA RM L57D16a, 1957.

2. Morgan, Homer G., and Miller, Robert W.: Flutter Tests of Some Simple Models at a Mach Number of 7.2 in Helium Flow. NASA MEMO 4-8-59L, 1959.

3. Lauten, William T., Jr., Levey, Gilbert M., and Armstrong, William O.: Investigation of an All-Movable Control Surface at a Mach Number of 6.86 for Possible Flutter. NACA RM L58B27, 1958.

4. Gibson, Frederick W., and Mixson, John S.: Flutter Investigation at a Mach Number of 7.2 of Models of the Horizontal- and Vertical-Tail Surfaces of the X-15 Airplane. NASA MEMO 4-14-59L, 1959.

5. Ashley, Holt, and Zartarian, Garabed: Piston Theory - A New Aerodynamic Tool for the Aeroelastician. Jour. Aero. Sci., vol. 23, no. 12, Dec. 1956, pp. 1109-1118.

6. Cunningham, H. J.: Lift and Moment on Thin Arrowhead Wings With Supersonic Edges Oscillating in Symmetric Flapping and Roll and Application to the Flutter of an All-Movable Control Surface. NACA TN 4189, 1958.

7. Nelson, Herbert C.: Lift and Moment on Oscillating Triangular and Related Wings With Supersonic Edges. NACA TN 2494, 1951.

8. Woolston, Donald S., and Runyan, Harry L.: On the Use of Coupled Modal Functions in Flutter Analysis. NACA TN 2375, 1951.

9. Woolston, Donald S., and Runyan, Harry L.: Appraisal of Method of Flutter Analysis Based on Chosen Modes by Comparison With Experiment for Cases of Large Mass Coupling. NACA TN 1902, 1949.

TABLE I

MODEL PARAMETERS

Model	Airfoil section	Pitch-axis location, fraction of root chord	Leading-edge sweep angle, deg	Center-of-gravity position		Mass, slugs	Moment of inertia about pitch axis, slug-ft^2	Natural frequency			
				Aft of pitch axis, in.	Outboard of root chord, in.			Flapping, cps	Pitching, cps	Second bending, cps	Camber, cps
1	Wedge	0.60	60	0.41	1.29	5.48×10^{-3}	8.24×10^{-5}	27.4	62.2	225	372
2			65	.43	1.04	4.29	6.24	34.0	69.0	334	403
3			70	.42	.91	3.36	4.88	41.8	76.0	383	412
4			75	.40	.72	2.60	3.71	55.2	89.6	498	385
5			80	.39	.67	1.69	2.42	72.0	106.6	810	392
6		.65	60	.13	1.28	5.29	7.38	27.5	57.5	250	375
7			65	.11	1.01	4.40	6.01	35.0	64.6	310	386
8			70	.11	.86	3.50	4.77	43.2	72.6	380	435
9			75	.14	.76	2.60	3.45	56.2	83.8	580	500
10			80	.13	.65	1.68	2.27	72.9	95.6	820	395
11	Double wedge	.60	60	.45	1.25	5.44	8.09	27.7	62.5	225	415
12			65	.40	1.06	4.25	6.26	33.3	68.4	298	408
13			70	.42	.84	3.57	5.06	43.2	79.6	395	485
14			75	.44	.72	2.57	3.72	54.0	90.0	550	450
15			80	.36	.57	1.72	2.33	75.4	110.0	850	430
16		.65	60	.09	1.27	5.40	7.49	27.8	58.6	260	420
17			65	.11	1.08	4.23	5.78	33.3	63.2	310	430
18			70	.13	.94	3.31	4.51	41.8	70.4	395	470
19			75	.06	.75	2.47	3.32	54.0	81.5	510	480
20			80	.06	.65	1.73	2.28	76.9	102.6	850	450

TABLE II

RESULTS

Model	Experimental					Theoretical					
						Coupled-mode piston theory		Uncoupled-mode piston theory		Uncoupled-mode lifting-surface theory	
	Dynamic pressure, lb/sq ft	Density slugs/cu ft	Speed of sound, ft/sec	Frequency ratio[a]	Stiffness-altitude parameter	Frequency ratio[a]	Stiffness-altitude parameter	Frequency ratio[a]	Stiffness-altitude parameter	Frequency ratio[a]	Stiffness-altitude parameter
1	1,871	1.086×10^{-4}	839	0.711	6.01	0.740	7.38	0.797	5.52	0.500	7.99
2	2,190	1.278	836	.733	6.08	.737	7.00	.824	5.75	.625	7.41
3	2,256	1.319	836	.789	6.61	.773	6.33	.850	6.12	.742	7.41
4	2,679	1.651	814	.817	7.30	.803	6.21	.883	7.21	1.003	7.76
5	3,652	2.238	816	.854	7.42	.881	7.34	.903	7.32	1.462	7.02
6	2,251	1.301	841	.696	4.99	.729	5.73	.715	4.28	.513	5.67
7	2,641	1.621	816	.740	5.25	.751	5.58	.751	4.91	.670	5.68
8	2,562	1.529	826	.774	6.04	.774	5.45	.784	5.55	.767	6.24
9	3,520	2.083	831	.805	5.99	.808	5.70	.804	5.90	1.077	5.83
10	[b]5,499	[b]3.388	[b]814	-----	[b]5.40	.862	6.23	.843	6.37	1.753	5.25
11	1,701	1.002	833	.685	6.31	.689	7.66	.812	6.56	.477	8.05
12	1,674	.994	829	.722	6.83	.718	7.48	.846	6.67	.550	7.99
13	2,106	1.254	828	.717	7.35	.735	7.53	.861	7.73	.726	8.38
14	2,350	1.367	838	.769	7.82	.766	7.50	.899	8.08	.913	8.26
15	3,243	1.949	824	.823	8.19	.821	8.47	.900	8.16	1.370	7.57
16	1,758	1.040	831	.669	5.80	.704	6.57	.750	5.76	.455	6.40
17	1,819	1.165	798	.718	6.07	.723	6.61	.768	5.68	.575	6.30
18	1,983	1.185	827	.751	6.47	.756	6.78	.792	6.04	.667	6.08
19	2,218	1.308	832	.798	7.12	.801	7.17	.820	6.61	.852	6.34
20	4,475	2.643	831	.828	6.55	.849	8.07	.850	7.73	1.539	5.90

[a]Ratio of flutter frequency to pitch frequency.

[b]Maximum tunnel operating conditions.

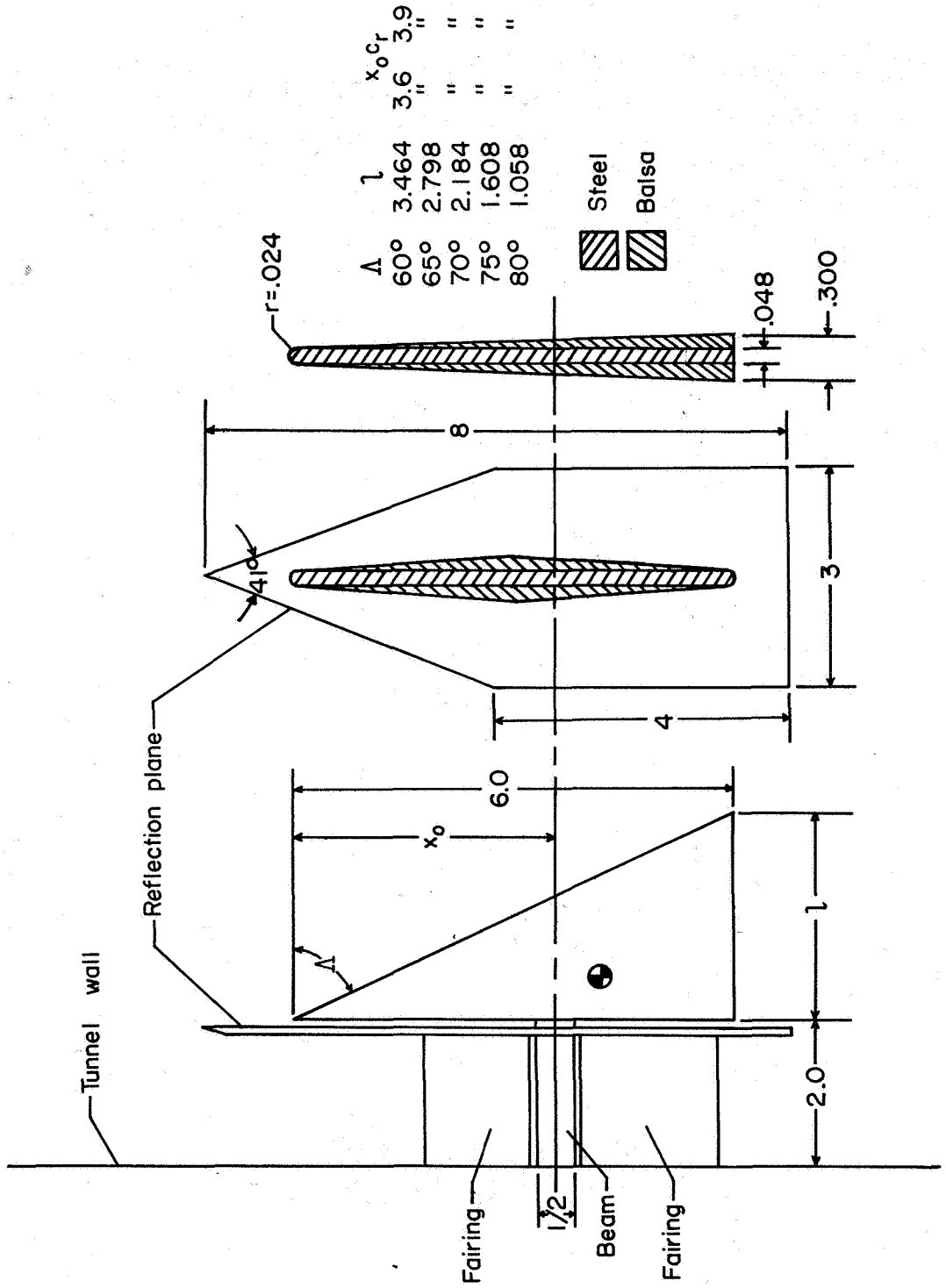

Figure 1.- Sketches of models. Dimensions are in inches.

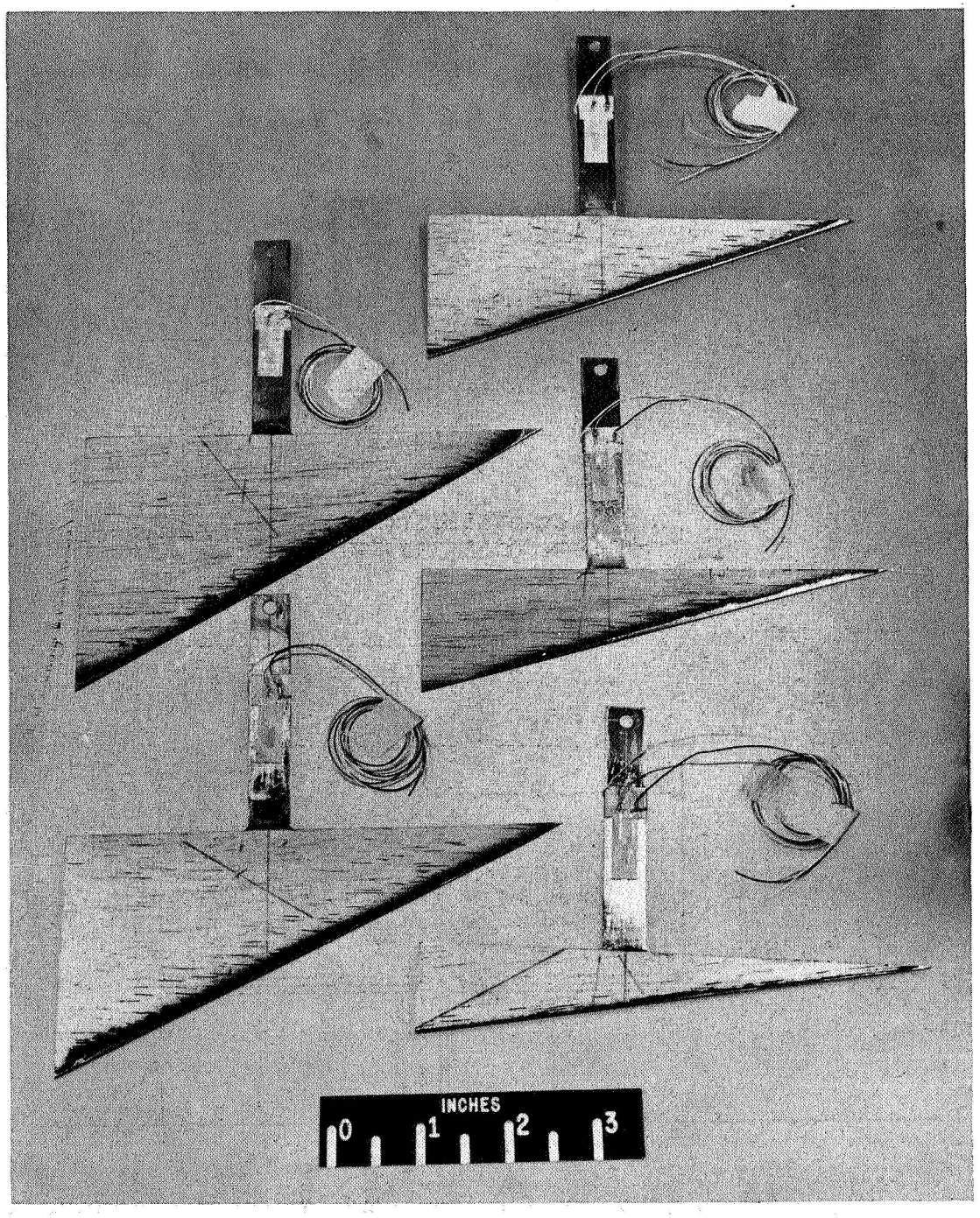

L-59-5247

Figure 2.- Photographs of wedge models with $x_o = 0.60$.

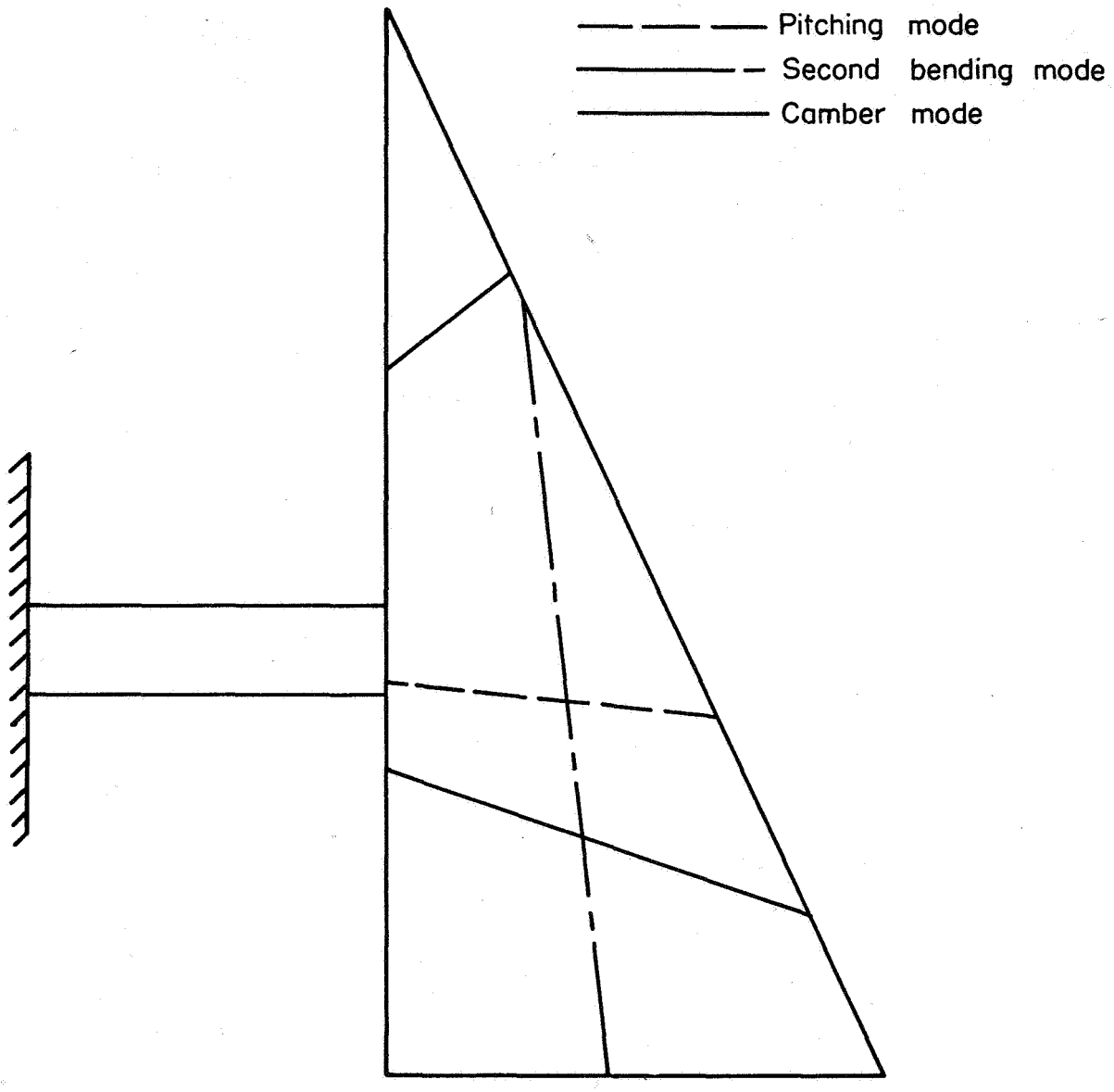

Figure 3.- Typical nodal patterns.

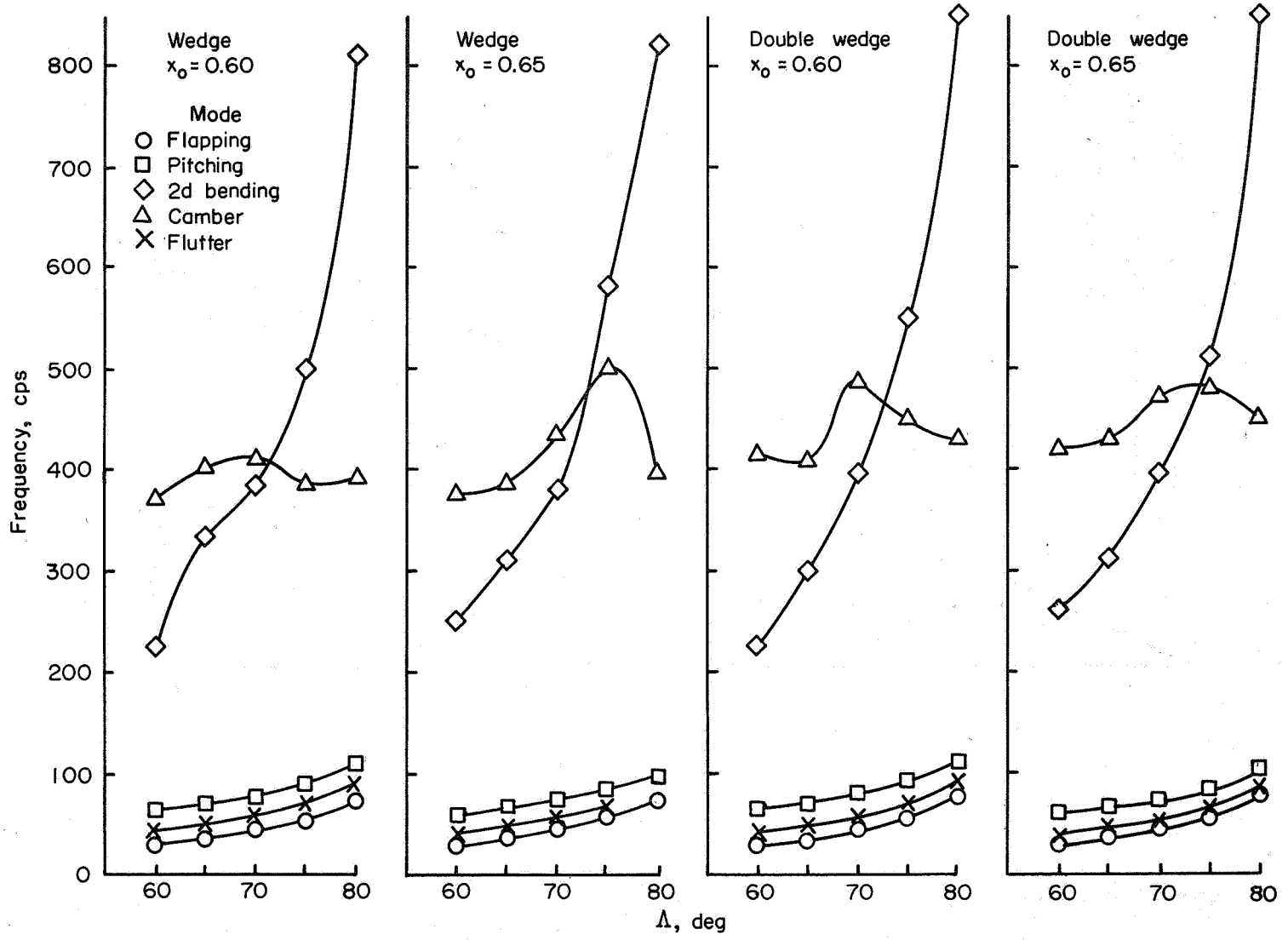

Figure 4.- Frequency characteristics of models.

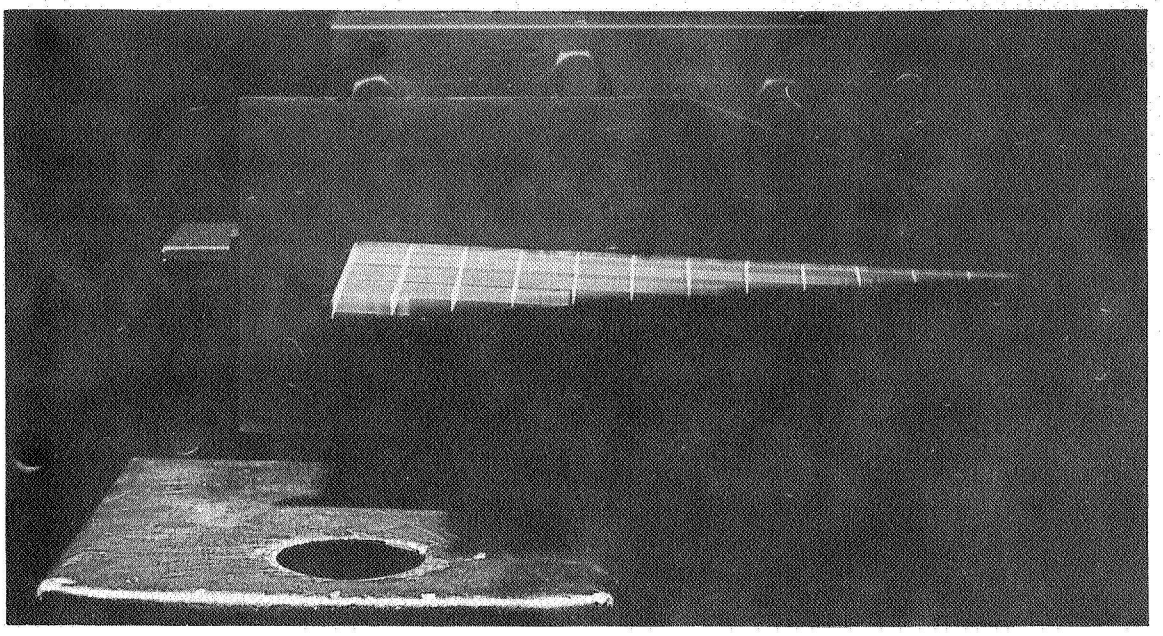

(a) Wedge model vibrating in flapping mode. $\Lambda = 70^{\circ}$.

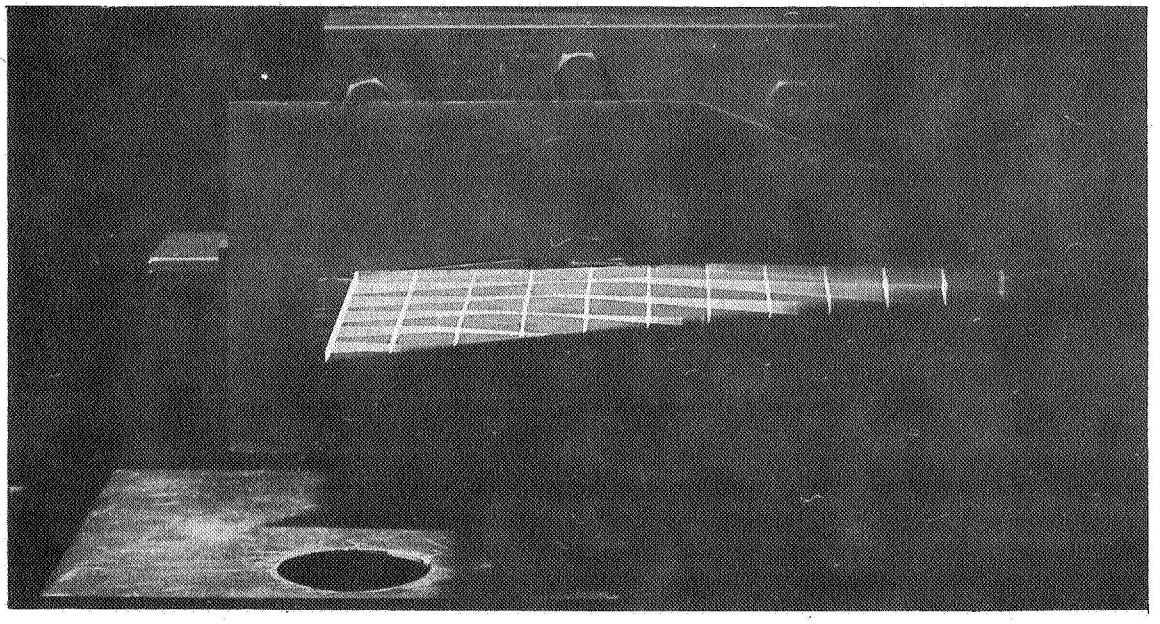

L-60-2487

(b) Double-wedge model vibrating in pitching mode. $\Lambda = 65^{\circ}$.

Figure 5.- Arrangement for determining modal deflections.

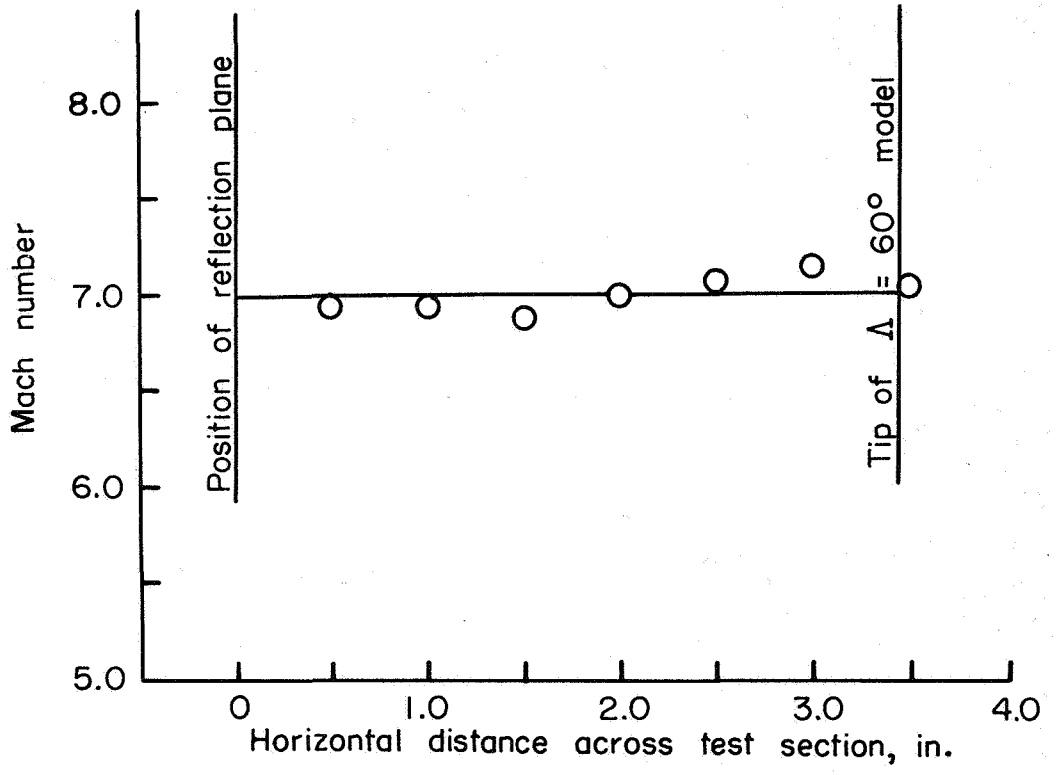

Figure 6.- Mach number distribution across test section.

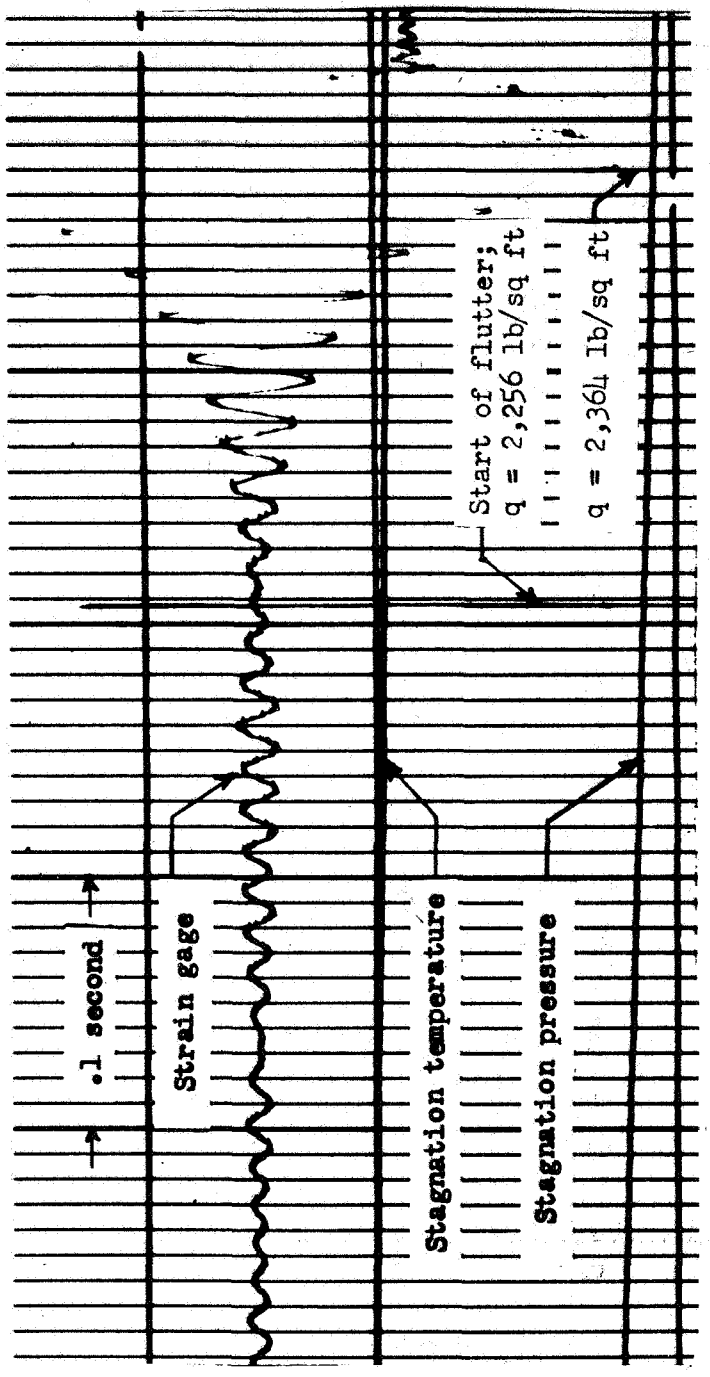

Figure 7.- Sample record showing flutter.

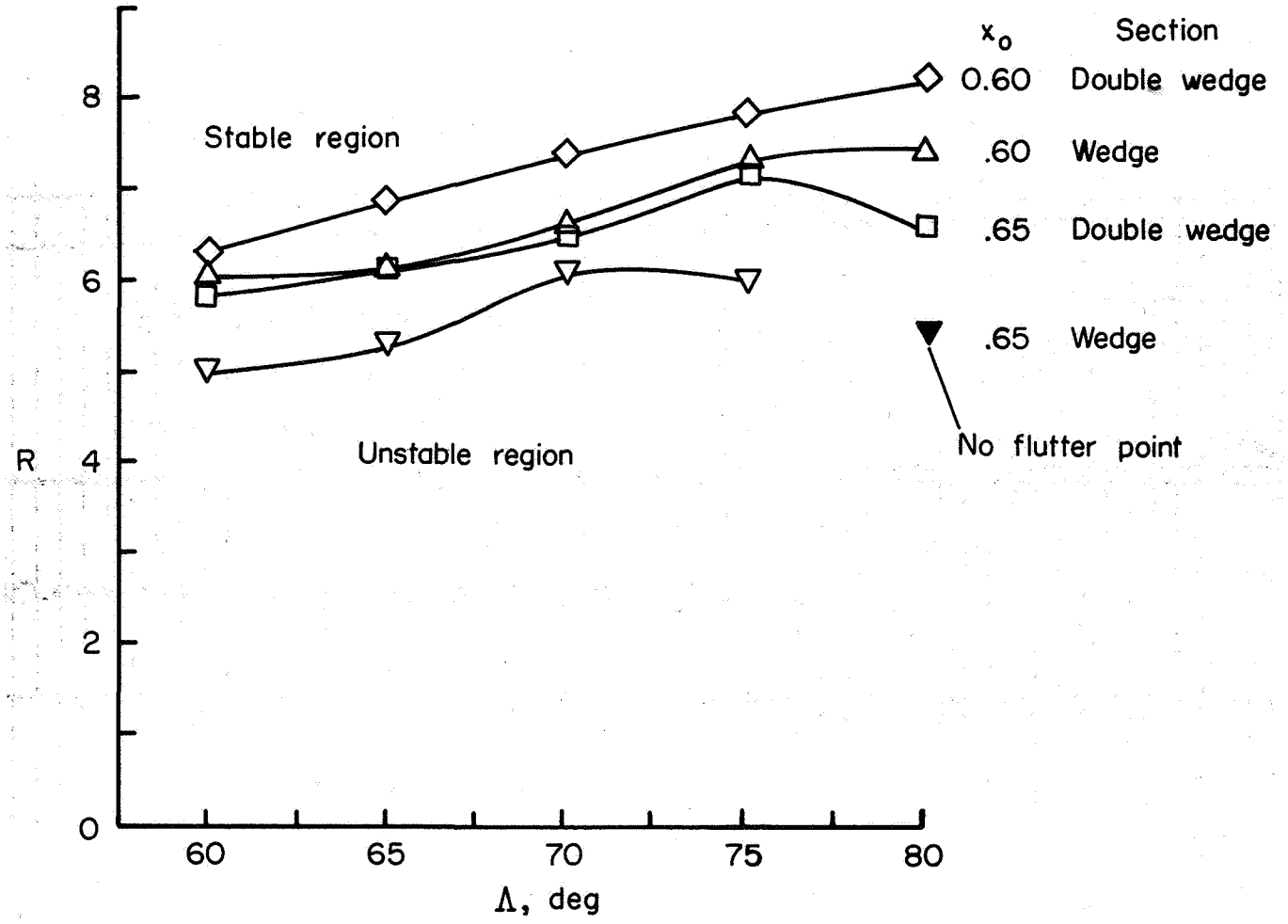

Figure 8.- Variation of experimental stiffness-altitude parameter R with leading-edge sweepback angle Λ.

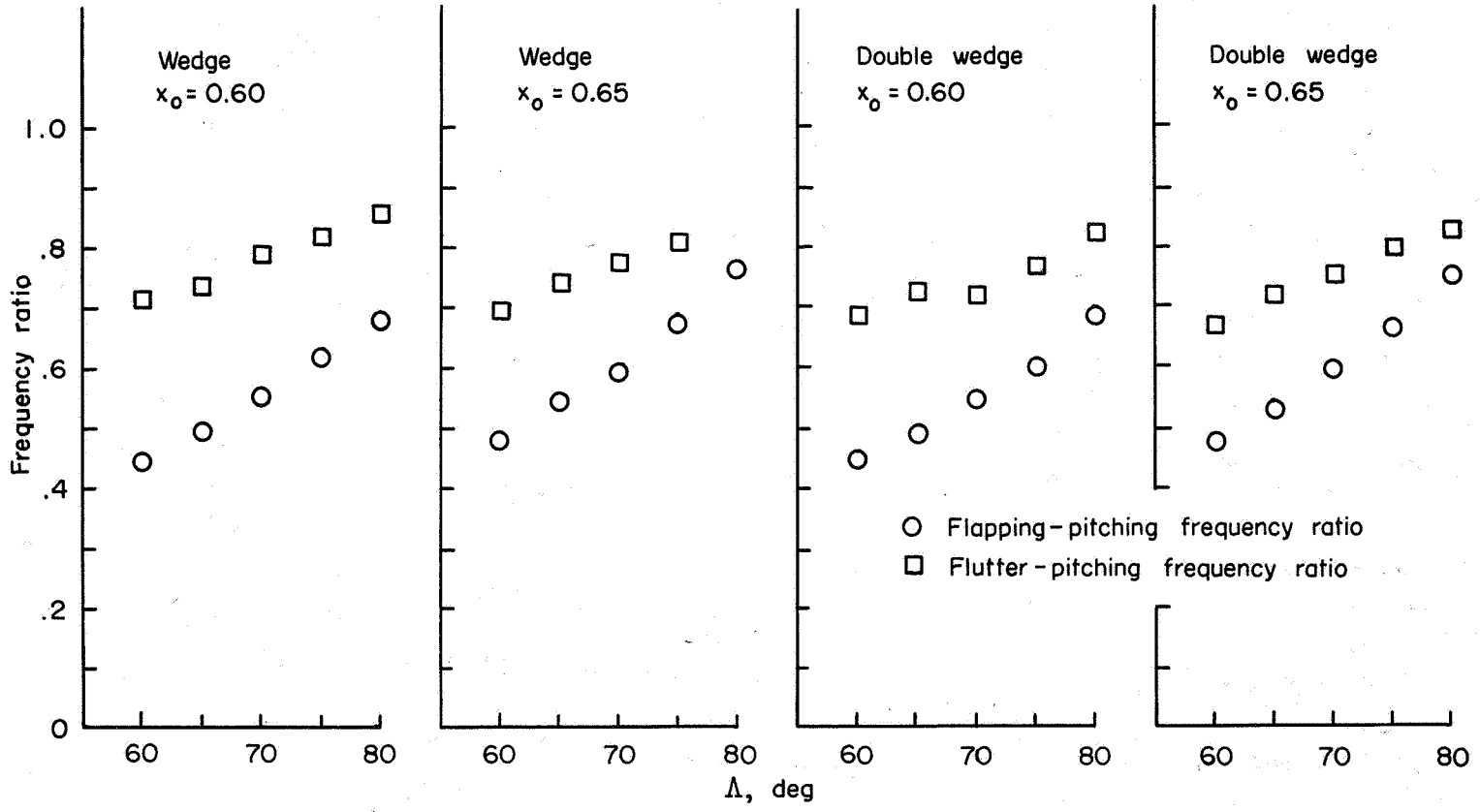

Figure 9.- Variation of experimental frequency ratios with leading-edge sweepback angle Λ.

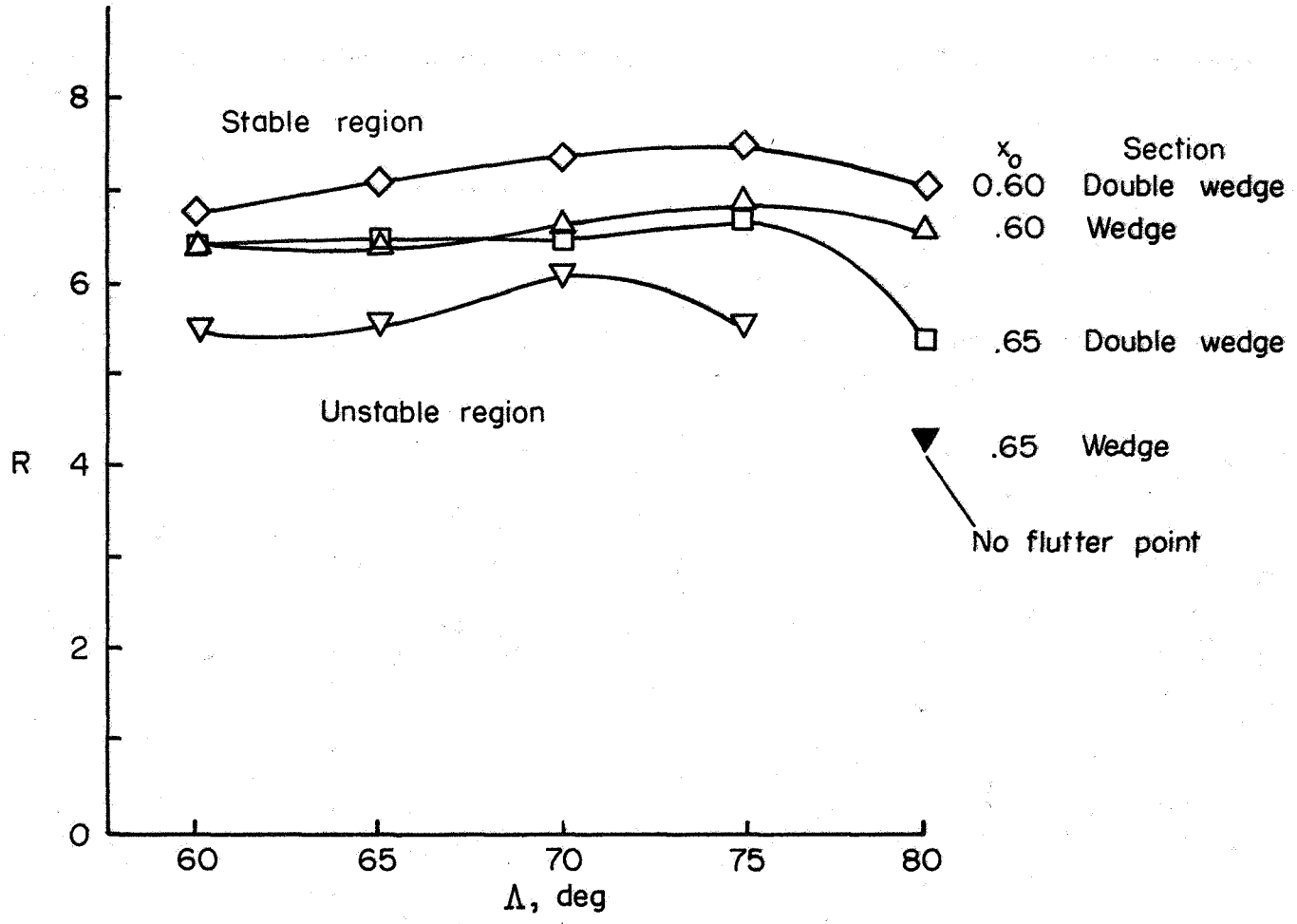

Figure 10.- Variation of experimental adjusted stiffness-altitude parameter R with leading-edge sweepback angle Λ.

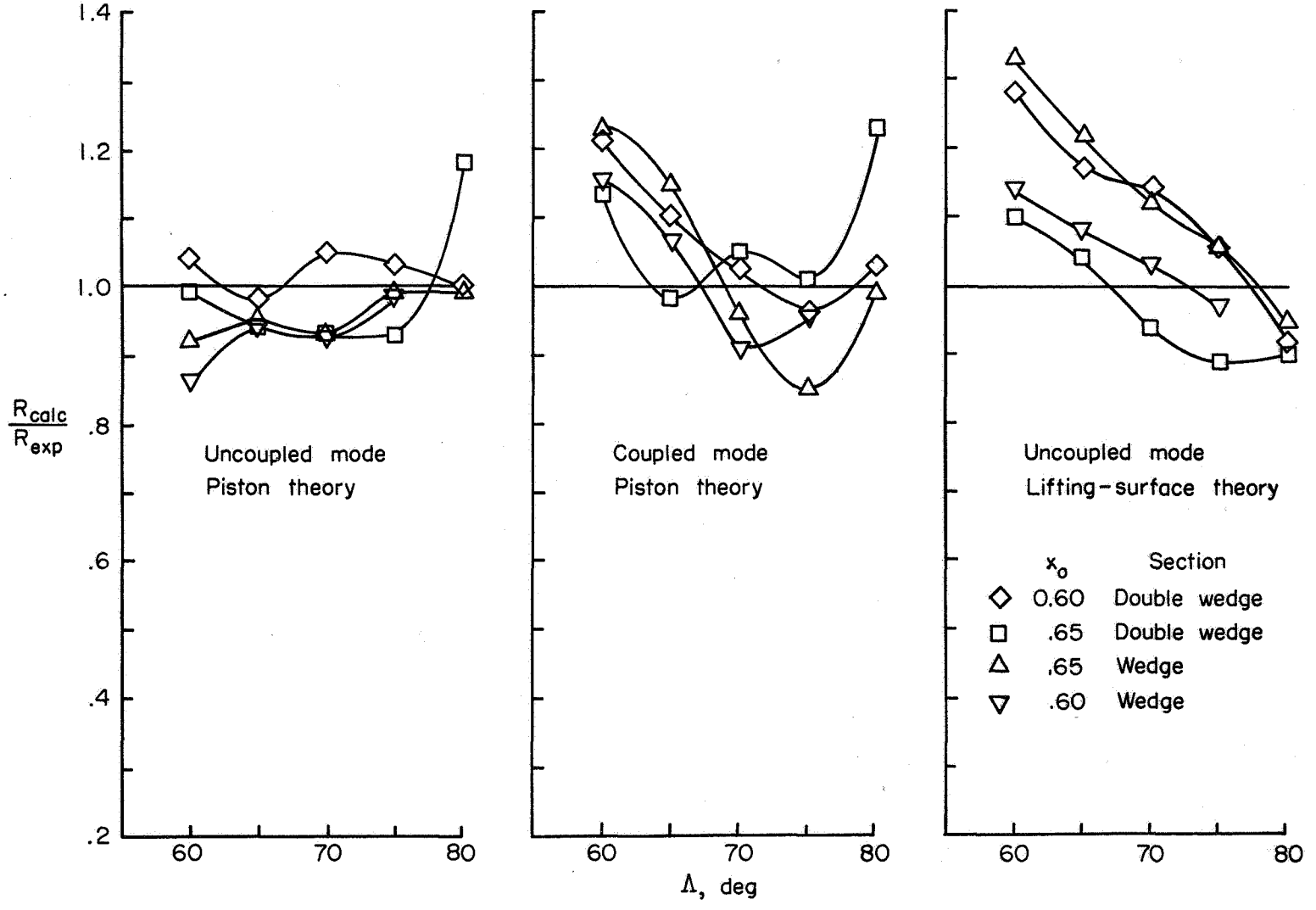

Figure 11.- Variation of the ratio of calculated to experimental stiffness-altitude parameter R with leading-edge sweepback angle Λ.